Atmos. Chem. Phys. Discuss., 5, 7247–7282, 2005
www.atmos-chem-phys.org/acpd/5/7247/
SRef-ID: 1680-7375/acpd/2005-5-7247
European Geosciences Union

Atmospheric Chemistry and Physics Discussions

Seasonal cycles and variability of O_3 and H_2O in the UT/LMS during SPURT

M. Krebsbach[1], C. Schiller[1], D. Brunner[2], G. Günther[1], M. I. Hegglin[2], D. Mottaghy[3], M. Riese[1], N. Spelten[1], and H. Wernli[4]

[1]Institute for Chemistry and Dynamics of the Geosphere: Stratosphere, Research Centre Jülich GmbH, Jülich, Germany
[2]Institute for Atmospheric and Climate Science, Federal Institute of Technology, Zurich, Switzerland
[3]Applied Geophysics, RWTH Aachen University, Aachen, Germany
[4]Institute for Atmospheric Physics, University of Mainz, Mainz, Germany

Received: 13 July 2005 – Accepted: 11 August 2005 – Published: 22 August 2005

Correspondence to: M. Krebsbach (m.krebsbach@fz-juelich.de)

Abstract

Airborne high resolution in situ measurements of a large set of trace gases including ozone (O_3) and total water (H_2O) in the upper troposphere and the lowermost stratosphere (UT/LMS) have been performed above Europe within the SPURT project. With its innovative campaign concept, SPURT provides an extensive data coverage of the UT/LMS in each season within the time period between November 2001 and July 2003.

Ozone volume mixing ratios in the LMS show a distinct spring maximum and autumn minimum, whereas the O_3 seasonal cycle in the UT is shifted by 2 to 3 month later towards the end of the year. The more variable H_2O measurements reveal a maximum during spring/summer and a minimum during autumn/winter with no phase shift between the two atmospheric compartments.

For a comprehensive insight into trace gas composition and variability in the UT/LMS several statistical methods are applied using chemical, thermal and dynamical vertical coordinates. In particular, 2-dimensional probability distribution functions serve as a tool to transform localised aircraft data to a more comprehensive view of the probed atmospheric region. It appears that both trace gases, O_3 and H_2O, reveal the most compact arrangement and are best correlated in the view of potential vorticity (PV) and distance to the local tropopause, indicating an advanced mixing state on these surfaces. Thus, strong gradients of PV seem to act as a transport barrier both in the vertical and the horizontal direction. The alignment of trace gas isopleths reflects the existence of a year-round extra-tropical tropopause transition layer. The SPURT measurements reveal that this layer is mainly affected by stratospheric air during winter/spring and by tropospheric air during autumn/summer.

Mixing entropy values for O_3 and H_2O in the LMS appear to be maximal during spring and summer, respectively, indicating highest variability of these trace gases during the respective seasons.

ACPD

5, 7247–7282, 2005

1. Introduction

Ozone and water vapour are important absorbers of solar irradiance and emitters/absorbers of terrestrial radiation. Both species have direct and indirect effects on radiative forcing and/or photolysis rates and play therefore a decisive role for the radiative budget of several atmospheric regions, for chemistry and climate. They are further suitable trace gases to investigate and understand transport and mixing processes, especially in the region of the upper troposphere and lowermost stratosphere (UT/LMS). This part of the atmosphere is to a large extent affected by dynamics, and in particular by bi-directional stratosphere-troposphere exchange. Trace gas distributions in the UT/LMS depend strongly on the interaction between dynamical and chemical processes near the tropopause. Changes in the chemical composition of the UT/LMS have strong impact on atmospheric radiation. A detailed understanding of the trace gas distributions, their variability, underlying processes and transport mechanisms of natural and anthropogenic emissions is crucial for climate prediction and radiative feedback mechanisms, in particular, when considering global warming scenarios (e.g. Lindzen, 1990; Rind et al., 1991; Inamdar and Ramanathan, 1998) and in climate simulations (e.g. McLinden et al., 2000). The UT/LMS and especially the tropopause region is thus of significant scientific interest.

Several data sets of satellite instruments have been analysed to infer seasonal distributions of ozone and water vapour in the LMS as well as connected transport mechanisms. From SAGE II measurements, Pan et al. (1997) inferred ozone and water vapour distributions in the LMS and compared them to MLS and ER-2 measurements (Pan et al., 2000). MLS water vapour data was further investigated by Stone et al. (2000) regarding climatological aspects as well as spatial and temporal variability. Randel et al. (2001) and Park et al. (2004) used HALOE data to derive seasonal variation of water vapour in the LMS. Furthermore, ozone and water vapour data in the UT and LMS from POAM III measurements were analysed by Prados et al. (2003) and Nedoluha et al. (2002), respectively. Satellite observations are thus a powerful tool

ACPD
5, 7247–7282, 2005

for a global data coverage of the whole atmosphere. However, there are several disadvantages and restrictions given by nature and technology, in particular, the limited spatial resolution. Due to the restrictions and the lack of satellite data in the UT/LMS, the tropopause region is rather under-sampled. Highly accurate and resolved observations of the UT/LMS can only be achieved with in situ measurements. For instance, Strahan (1999) analysed ozone data from ER-2 flights in the potential temperature region between 360 K and 530 K. Anyhow, aircraft measurements are commonly quite sporadically distributed in time and space. For such purposes, projects like MOZAIC (e.g. Marenco et al., 1998), NOXAR (e.g. Brunner et al., 1998) or CARIBIC (e.g. Brennikmeijer et al., 2005) use commercial and passenger aircraft to measure routinely chemical species. However, thereby only the lower part of the LMS is reached.

A cutting edge for a new concept of aircraft campaigns was introduced by the very successful project SPURT (German: SPURenstofftransport in der Tropopausenregion, trace gas transport in the tropopause region). Within the European sector (30° E to 30° W, 30° N to 80° N) an extensive and continuous high quality data coverage of the UT and LMS in each season was obtained. Using a Learjet 35A a total of eight campaigns, evenly distributed in time between November 2001 and July 2003, were performed. Depending on meteorological conditions, the aircraft's ceiling altitude is about 14 km and thus allows for sampling in the LMS during all seasons, even at subtropical latitudes. The SPURT measurements between the 280 K and 380 K isentropes thus contribute significantly to the data coverage in the whole extra-tropical LMS above Europe. A description of the project strategy, its aims, performance and instrumentation is given in an overview paper by Engel et al. (2005).

The purpose of this work is to analyse the seasonality and variability of ozone (O_3) and total water (H_2O) in the UT/LMS as measured during the SPURT project. After a short description of these trace gas measurements, the seasonal cycles of O_3 and H_2O are discussed. Several statistical perspectives are used to investigate trace gas variability and implications for the trace gas distribution in the probed atmospheric region.

2. The SPURT O_3 and H_2O data

During the SPURT campaigns, O_3 was measured with UV absorption by the JOE instrument (Jülich Ozone Experiment) (Mottaghy, 2001). For most flights, i.e. from the third campaign on, O_3 was additionally measured by a chemiluminescence detector ECO-Physics CLD 790-SR (Hegglin, 2004). Intercomparison of both instruments results in high consistency (Hegglin, 2004; Engel et al., 2005). However, in the presented analyses here the JOE data is preferably considered and ECO data are only used if no JOE data are available. Total water, i.e. the sum of vapour and vaporised ice, was measured with the photofragment-fluorescence technique by the FISH instrument (Fast In situ Stratospheric Hygrometer) (Zöger et al., 1999). The instruments JOE, ECO and FISH have a time resolution of 10, 1, 1 s, and an accuracy of 5, 5, 6%, respectively. Due to the different integration times of the single instruments the measurement data was analysed as 5 s data. Thereby, the JOE data was interpolated to the centre interval, measurements with a higher sampling rate were averaged over each 5 s. For an average aircraft flight speed of 150 to 200 m s^{-1} this results in a mean spatial resolution of 0.75 to 1.00 km. For a complete listing of the Learjet payload, data availability, and for details about the processing of the whole SPURT data set see Engel et al. (2005).

Figure 1 gives an impression of the obtained coverage of O_3 and/or H_2O measurements during SPURT in the geographical and potential temperature space. The map in the left panel reflects the number of measurements in a 1° longitude × 1° latitude bin. Each campaign consisted of a minimum of 2 flight days. On one day southbound and on the other day northbound flights were performed from and back to the Learjet basis Hohn (9.53° E, 54.31° N, northern Germany). The contours clearly accentuate the basis in northern Germany as well as the two main inter-stations, Faro in southern Portugal for the southbound flights and Tromsø in Norway for the northbound flights. Slow ascents and descents in these regions result in a large number of measurements there. Each season (autumn, winter, spring, and summer, corresponding to the months SON, DJF, MAM, and JJA) was investigated with two campaigns.

ACPD
5, 7247–7282, 2005

The right panel of Fig. 1 shows frequency distributions of data points in potential temperature intervals from 280 K to 380 K in steps of 10 K. Potential temperature (Θ) is calculated from avionic measurements of pressure (p) and temperature (T). It indicates winter and spring with more than 23 000 and 25 000 data points, respectively, as the best captured seasons for O_3 and H_2O. With more than 19 000 data points also the autumn and summer season are probed quite well. The tail at the lower Θ values between 280 K and 310 K is a result of sampling, since the inlet of the FISH instrument was only opened at altitudes higher than a pressure value of ≈400 hPa. Similarly, the JOE instrument provides high qualitative data rather at altitudes above that pressure level. The frequency distributions in the Θ space reflects the SPURT concept of the flight profiles. Slow ascents and descents allowed for accurately resolved slant vertical profiles. Within each mission two flight legs at rather constant pressure altitude were performed, one near and the other above the tropopause (cf. numbers of data points within 320 K and 340 K and 350 K and 370 K, respectively). Due to fuel consumption and thus lower mass of the aircraft, at the end of each mission a climb to maximum altitude (>370 K) was performed to sample generally undisturbed stratospheric background air. The altitude flight profile was mirrored on the mission back to Hohn to sample the meteorological condition in two different height regimes.

To place the measurements in a meteorological context, ECMWF (European Centre for Medium-Range Weather Forecasts) analyses with a time resolution of 6 h and a grid resolution of $1^\circ \times 1^\circ$ in longitude and latitude on 21 pressure levels between 1000 and 1 hPa are used. Each analysis data set was interpolated to 25 isentropic surfaces located between 280 K and 400 K in steps of 5 K. On these isentropes potential vorticity (PV) is obtained by spatial and temporal interpolation to the flight tracks. The diagnosis of PV from meteorological data fields is affected by errors (e.g. Beekmann et al., 1994; Good and Pyle, 2004). The procedure of data assimilation will remove obvious observational errors (Hollingsworth and Lönneberg, 1989). Anyhow, the accuracy in calculating PV is sensitive to the horizontal and vertical resolution and, in particular, small-scale meteorological features like tropopause folds are hardly represented in de-

tail in the meteorological analyses. In contrast, in situ measurements have a much finer resolution and can therefore resolve small-scale features. This has to be considered when correlating model derived quantities with in situ measurements (cf. Sect. 4).

3. Seasonal cycles of O_3 and H_2O in the UT and LMS

In order to derive seasonal cycles of O_3 and H_2O in the UT and LMS, PV is used to categorise air parcels. Since PV increases with height and latitude in the northern hemisphere, it is used here to split the data set into atmospheric subsets. Detailed analyses of vertical profiles during ascents and descents reveal a PV value of 2.0 to 2.5 PVU (1 PVU=10^{-6}m^2 s^{-1} K kg^{-1}, according to Hoskins et al., 1985) as representative for the location of the extra-tropical tropopause during SPURT (e.g. Hoor et al., 2004; Krebsbach, 2005; Hegglin et al., in preparation[1]). Potential vorticity values lower than 1 PVU are therefore assumed to denote air of the (upper) troposphere, values within the range 1–3 PVU air of the tropopause region, and higher values reflect an increasing stratospheric character of the probed air.

3.1. O_3 in the UT and LMS

In Fig. 2 monthly median O_3 volume mixing ratios (VMRs) in different PV domains, characteristic for specific regions of the atmosphere, are shown as measured during SPURT. Thereby, a box plot graphing is used, showing centring (median), spread (25 and 75 quartiles), and distribution (minimum and maximum). Thus, an accurate impression of the central tendency and variability of O_3 is possible. Considering the complete data set, the seasonal cycle of O_3 in the (upper) troposphere shows a minimum during winter and a broad spring to summer maximum. There exists a number

[1]Hegglin, M. I., Brunner, D., Peter, Th., Hoor, P., Fischer, H., Staehelin, J., Krebsbach, M., Schiller, C., Parchatka, U., and Weers, U.: Measurements of NO, NO_y, N_2O, and O_3 during SPURT: Seasonal distributions and correlations in the lowermost stratosphere.

of regions showing a broad summer maximum in tropospheric ozone. The existence of such a maximum is often associated with photochemical production (e.g. Logan, 1985). Thereby, O_3 is formed by reactions involving volatile organic compounds and nitrogen oxide (NO_x), driven by solar radiation. Many of these regions are continental and influenced by pollution (e.g. Logan, 1989; Scheel et al., 1997). Also in the free troposphere, a broad spring to summer maximum was observed (e.g. Logan, 1985; Schmitt and Volz-Thomas, 1997). Beekmann et al. (1994) showed based on ozone sonde data from Observatoire de Haute-Provence (OHP) that the seasonal variation of tropospheric O_3 is characterised by a large maximum during spring and summer. Furthermore, LIDAR and ozone sonde measurements from OHP from 1976 to 1995 give evidence for a shift from a spring maximum to a spring/summer maximum in the free troposphere (Ancellet and Beekmann, 1997). The observed broad spring/summer O_3 maximum during SPURT in the UT with a slight shift towards spring is furthermore in accordance with results from Brunner et al. (2001).

Most variable O_3 VMRs are present during spring. During this season the influence of the large-scale downward motion is most prominent (Appenzeller et al., 1996). Also the net O_3 flux across the extra-tropical tropopause has a peak during spring to early summer, primarily affected by the outward O_3 flux of the LMS through the tropopause (Logan, 1999). Thus, the already enhanced tropospheric O_3 VMRs during spring seem to be effected by the downward transport of O_3-rich stratospheric air during that season.

Measurements at Mace Head, Ireland, illustrate a clear spring O_3 maximum (Derwent et al., 1998). However, the appearance of a spring maximum in the O_3 seasonal cycle in the northern hemisphere troposphere is heavily debated (cf. review by Monks, 2000). Regarding northbound and southbound flights during SPURT separately (not shown here), the maximum in tropospheric O_3 VMRs for higher latitudes occurs during late spring and is shifted to late summer further south (cf. Krebsbach, 2005). This is in agreement with results of Scheel et al. (1997) from low-altitude and mountain sites between 28–79° N. Further, Hough (1991) showed by 2-dimensional model studies

the general maximum of O_3 precursors like NO_x, carbon monoxide, and hydrocarbons in the free troposphere at middle and higher latitudes during winter and spring, which is in accordance with the slight shift towards spring observed during the northern SPURT flights. As mentioned before, additionally a contribution to higher O_3 VMRs in the UT during spring is presumably affected by a contribution of O_3-rich air due to stratosphere-to-troposphere transport. The observed maximum in O_3 VMRs during summer is possibly a result of in situ photochemical production (e.g. Logan, 1985; Haynes and Shepherd, 2000) since photochemical activity is expected to be highest during this period (e.g. Liu et al., 1987).

For higher PV values, in the LMS, a clear spring maximum and autumn minimum is evident with a peak-to-peak amplitude of ≈400 ppbv O_3 within the PV range of 8–9 PVU. The ozone build-up in this atmospheric region occurs during winter as a consequence of poleward and downward transport, since the lifetime of O_3 is long with respect to chemical loss (e.g. Holton et al., 1995) and is largely controlled by dynamics (Logan, 1999). The observed spring maximum in the LMS over Europe during SPURT is most probably due to the downward advection of high O_3 VMRs by the stratospheric winter/spring Brewer-Dobson circulation, in accordance with e.g. Logan (1985), Austin and Follows (1991), Oltmans and Levy II (1994), Haynes and Shepherd (2000), Prados et al. (2003). Ozone VMRs fall off from March to October with a maximum decrease rate within May to August. Much of this decrease is presumably caused by the change in tropopause height and transport mechanisms. On the basis of observations of SAGE II, Pan et al. (1997) and Wang et al. (1998) assumed that isentropic cross-tropopause inflow of tropospheric air into the LMS influences the seasonal cycle of O_3 (and H_2O, see Sect. 3.2) in that atmospheric region, especially during summer. A maximum of quasi-isentropic inflow into the LMS during summer was also identified in model studies by Chen (1995, 2-dimensional) and Eluszkiewicz (1996, 3-dimensional). Enhanced content of tropospheric air in September compared to May was identified by Ray et al. (1999) from balloon-borne chlorofluorocarbons and water vapour measurements, which was also thought to be owing to quasi-isentropic

in-mixing of tropospheric air. The seasonal cycle of O_3 in the extra-tropics therefore differs between the UT and the LMS. The transition region between the troposphere and the stratosphere (1–3 PVU) is rather influenced by the troposphere. However, just above the tropopause layer (4–5 PVU) the stratospheric signal becomes dominant.

Amplitudes of O_3 VMRs grow with increasing PV. Regarding the progression of O_3 VMRs through surfaces of increasing PV, the most prominent increase is apparent during winter and spring, whereas during summer and autumn the gradients are comparably weak. Since in Fig. 2 rather dynamically similar air parcels are considered and PV exhibits a transport barrier (cf. e.g. Krebsbach et al., a, in preparation[2], and Hegglin et al.), the lower O_3 gradients with respect to PV surfaces during summer and autumn suggest an intensified transport of tropospheric air into the LMS during these seasons (cf. Sect. 3.2). Towards higher PV ranges (> 3 PVU), i.e. deeper in the LMS, tropospheric influence decreases which results in an increase in the slope (dO_3/dPV). The observed seasonal variation of the slope has a maximum of about 60–90 ppbv/PVU in April and a minimum of 10–30 ppbv/PVU in October. The results are comparable with findings from Beekmann et al. (1994) and Zahn et al. (2004).

3.2. H_2O in the UT and LMS

As ozone, water vapour shows a distinct gradient at the extra-tropical tropopause. Due to the temperature lapse rate and the decrease in pressure, water vapour VMRs decrease exponentially with height from the troposphere up to the tropopause region. Calculated averages of measurements that span the transition region between the UT and the LMS are dominated by moist air from below the tropopause.

In Fig. 3 monthly medians of H_2O measured during SPURT are depicted in the same manner as for O_3 (cf. Fig. 2). Based upon the annual cycle of tropopause temperatures

[2]Krebsbach, M., Schiller, C., Spelten, N., Günther, G.: Characteristics of the extra-tropical transition layer as derived from O_3 and H_2O measurements in the UT/LMS during SPURT: I. trace gas distributions and stratosphere-troposphere exchange, a.

ACPD
5, 7247–7282, 2005

(e.g. Hoinka, 1999) and resulting ice saturation VMRs, maximum H_2O VMRs in the tropopause region are expected during the summer, lowest during the winter months. The SPURT measurements show maximum H_2O VMRs in the (upper) troposphere (0–1 PVU) during the August 2002 campaign. However, the spring campaign in April 2003 shows a secondary maximum, whereas in May 2003 comparably low H_2O VMRs are apparent. This feature pervades through the whole considered PV categories and reflects the high variability of H_2O in the probed atmospheric region. Anyhow, the tendency of higher VMRs during summer and lower ones during winter and also autumn is present. Across the tropopause the strong gradient in H_2O is evident. When considering northbound and southbound flights separately, the southern tropopause region is slightly dryer. This is probably due to the higher influence of the dryer sub-tropical regions (see for instance Hoinka, 1999; Krebsbach, 2005).

In the LMS (>4 PVU) a clearer seasonal cycle in H_2O is apparent with a distinct maximum during summer and a minimum during autumn and winter. This is in agreement with previous in situ and remote observations (e.g. Mastenbrook and Oltmans, 1983; Foot, 1984; Oltmans and Hofmann, 1995; Dessler et al., 1995; Pan et al., 1997; Stone et al., 2000). In contrast to O_3, with increasing PV the H_2O VMRs as well as the amplitude of the annual cycle decreases (note the logarithmic ordinate). This indicates a more pronounced seasonal cycle of H_2O in the lower LMS.

Air in the so called “overworld” (Hoskins, 1991) is dehydrated as it is transported through the tropical cold trap. However, for a large extent of the performed SPURT campaigns H_2O VMRs are considerably enhanced compared to stratospheric background values of about 2–7 ppmv (e.g. Hintsa et al., 1994). Even in the upper considered PV ranges median H_2O VMRs during summer are about 30 ppmv. These VMRs are much higher than could solely be explained by entry of air into the stratosphere in the tropics (e.g. Foot, 1984; Nedoluha et al., 2002). Thus, values substantially greater than 7 ppmv are evidence for transport mechanisms of air into the LMS across the extra-tropical tropopause, and this signature is carried deep into the lower stratospheric region.

The variability of H_2O for observations in the tropopause region and in the stratosphere increases from autumn/winter towards summer (see also Sect. 4 and frequency distributions in Krebsbach, 2005). This suggests that the potential for transport of water through the tropopause is more effective and thus more important and significant during summer. This is especially relevant for long-term transport which is the combined effect of mass transport and the efficiency of freeze-drying. Hence, as already derived from the O_3 data, the LMS seems to be more influenced by the troposphere during summer than during winter which is in agreement with the discussed seasonal variability of water vapour in the LMS by e.g. Pan et al. (2000).

Whereas the O_3 maximum in the UT is approximately in phase with the H_2O maximum, it occurs about 2–3 months later (earlier) in the year as the O_3 maximum (minimum) in the LMS. A similar time lag was found by Pan et al. (1997) and Prados et al. (2003). Due to the large debate, especially concerning the often observed spring O_3 maximum at some northern hemisphere stations, it is further to investigate to what extent the correlation and/or anti-correlation of both trace gases could be attributed to dynamics or to chemistry. Anyhow, the seasonal cycles of O_3 and H_2O obtained during the SPURT campaigns underline the influence of two competing processes in the UT/LMS region: (i) subsidence of dry air from the overworld, which is primarily determined by the low tropical tropopause temperatures and transported by the large-scale Brewer-Dobson circulation (e.g. Holton et al., 1995), and (ii) direct transport of moist air of tropical, sub-tropical or mid-latitude origin across the extra-tropical tropopause (e.g. Dessler et al., 1995; Hintsa et al., 1998). As is apparent in Fig. 3, in contrast to the O_3 VMRs, the seasonal cycles of H_2O in the UT and LMS are roughly in phase with each other. This same seasonal course in both atmospheric compartments is a priori not clear. Whereas much of the air in the LMS has probably been transported into the stratosphere by the former process (i), it is likely that local vertical transport processes play a much larger role in determining H_2O in the UT and the lower LMS.

ACPD
5, 7247–7282, 2005

4. O_3 and H_2O in a view from different coordinates

The SPURT measurements covered a broad latitude range with different meteorological situations, often associated with small-scale phenomena (e.g. tropopause folds) and large-scale meridional advection of polar and/or sub-tropical and/or tropical air. The different dynamical impacts result in discontinuities and changes in the tropopause height, particularly in the vicinity of regions with high wind velocities, the jet streams, in the literature often referred to as the region of the "tropopause break". In order to get a comprehensive insight into distribution, spreading, ranging, and variability of the measured trace gases in the SPURT region, 2-dimensional probability distribution functions (PDFs) are determined by using chemical, thermal, and dynamical vertical coordinates. Moreover, it is interesting to investigate which coordinate is best correlated with a trace gas and where the most compact correlation appears. An accurate correlation helps to deduce and to assess transport processes and provides the possibility for transformation into related quantities (see e.g. Krebsbach et al., b, in preparation[3]).

4.1. Probability distribution functions

In several SPURT flights, distinct cross-tropopause exchange events and characteristic features for specific meteorological situations could be identified (e.g. Hegglin et al., 2004, Krebsbach et al., c, in preparation[4]). To obtain a compact view of the probed atmospheric region, PDFs are a tool to centralise the large number of measurements. As an advantage of the PDFs, all measurement data is considered, and averaging is minimised. Thus, outliers become more visible and the prominent structures and features are revealed (Ray et al., 2004).

[3]Krebsbach, M., Schiller, C., Spelten, N., Günther, G.: Characteristics of the extra-tropical transition layer as derived from O_3 and H_2O measurements in the UT/LMS during SPURT: II. extent and seasonal variation, b.

[4]Krebsbach, M., Schiller, C., Günther, G., Wernli, H.: Transport across the extra-tropical tropopause and impact on the H_2O content of the LMS, c.

ACPD
5, 7247–7282, 2005

In Fig. 4, PDFs of O_3 (left) and H_2O (right) as a function of the thermal vertical coordinate potential temperature for the spring season are depicted. For the distributions obtained for the other seasons it is referred to Krebsbach (2005). Ozone is binned by 20 ppbv, H_2O by 2 ppmv, and potential temperature by 5 K. The trace gas distributions are normalised to every bin of the thermal coordinate. This means, the colour coding reflects the probability in percent to measure a certain trace gas VMR at a certain potential temperature. Additionally, the mean and median value in each Θ bin is represented by the solid and dashed coloured line, respectively. While the mean is an appropriate measure of the central tendency for roughly symmetric distributions, it is misleading when applied to skewed distributions since it can greatly be influenced by extremes. In contrast, the median is less sensitive to outliers and may be more informative and representative for skewed distributions. All seasonal means and medians are displayed to compare to each other (red, blue, green, and orange for autumn, winter, spring, and summer, respectively).

High probabilities, reflected by the light grey/green shadings, are very scattered throughout the O_3 distribution and, although both parameters, Θ and O_3, can be considered as a vertical coordinate, no clear correlation is apparent. There is no symmetry around the mean or median values and multiple modes can be noted. Generally, an increase of O_3 VMRs with increasing Θ (height) is present, but the spreading of O_3 VMRs on levels with constant potential temperature, the isentropes, is considerably large, resulting in a funnel or wedge structure. However, the large scatter and spread in the O_3 distributions is expected, since the O_3 VMRs are largely dependent upon the location of the tropopause. The single flight missions extended over a large latitude range. Therefore, the variability of potential temperature at the tropopause location during each deployment along the flight path was sometimes quite large. For instance, on a flight from Hohn to Tromsø on 17 May 2002, the tropopause was located at 304 K in the vicinity of Tromsø and at 328 K near the campaign base Hohn, which is a variation of 24 K (see Krebsbach, 2005). However, also at higher isentropes, i.e. further away from the local tropopause, the spread in O_3 VMRs is very high.

The H_2O PDF shown here as well as the distributions for the other seasons (see Krebsbach, 2005) exhibit similar characteristics as those for O_3. The large variation of the tropopause location is transparent in the high amounts of H_2O VMRs below ≈340 K, where also in the course of means, and partly of the medians, at lower isentropes a strong kink is present. A more compact distribution is only apparent above ≈350 K, with the higher variability during the summer season. When shifting the mean H_2O VMRs for the summer PDF by ≈20 K towards lower isentropes, the shape of the mean line (orange) is quite similar to the mean line for the winter season (blue). The SPURT measurements are mainly concentrated in the atmospheric region above isentropes of ≈320 K. Thus, a strongest tropospheric influence during summer, as already mentioned in the previous section, is in agreement with the seasonally integrated mass flux through troposphere-to-stratosphere transport by Sprenger and Wernli (2003, their Fig. 3b).

The shapes of the trace gas PDFs for the winter and spring measurements are quite different from the distributions obtained for summer and autumn (see Krebsbach, 2005). Whereas the former show a rather steep distribution with rising O_3 VMRs and increasing Θ, the latter are more flat or show a prominent wedge structure towards higher isentropes. The large variability of trace gas VMRs, especially at higher isentropes (e.g. >400 ppbv O_3 at 360 K during all seasons) and the occurrence of several high probabilities on single isentropes, indicate that quasi-isentropic mixing is rather weak in this region.

The picture drawn on the basis of Θ changes significantly when shifting the thermal coordinate to a dynamic coordinate, namely PV. The corresponding trace gas PDFs are shown for all seasons in Fig. 5 with PV incremented in 0.5 PVU steps. As is directly evident, O_3 is much stronger correlated with PV than with Θ, which is rather an accurate height or correlation parameter in the undisturbed stratosphere. The ranging of O_3 VMRs on surfaces of PV is considerably suppressed when compared to the spreading on isentropes. Even the wedge structure in the autumn and summer distributions as a function of Θ is significantly reduced. The highest probabilities are mostly

centred in the distributions and symmetrically arranged around the mean or median O_3 VMRs in every PV bin. In the PV-PDFs, additionally the trace gas gradients in dependence of the coordinate are calculated within 2 PVU intervals. The O_3/PV-gradients are ≈2–4 times stronger in the 2–4 PVU range than within the interval 0–2 PVU. The means and medians show a slight kink in this range, indicating 2 PVU as a good proxy for the dynamically defined extra-tropical tropopause during the SPURT missions. Of course, the gradient is weaker during summer which is due to the annual cycle of O_3 in the UT and in the LMS. Thus, the distinct seasonal cycles of O_3 in both atmospheric compartments, UT and LMS, are clearly apparent.

For H_2O, the spreading in the PDFs is also reduced with PV as the reference coordinate. The kink due to the varying location of the local tropopause in the Θ space is not present in the PV space. Also above 2–3 PVU, i.e. within the tropopause region, the variation of H_2O VMRs on PV surfaces is significantly reduced. However, during summer the H_2O distribution is more compact when related to Θ.

As shown by the mean and medians, moreover the seasonal cycles of H_2O in the UT and LMS are reflected in the PDFs, with certainly higher VMRs during the summer months in the UT as well as in the LMS. The trace gas VMRs show a more compact distribution in a dynamical sense. In contrast to the spreading and distribution of several high probabilities on isentropic surfaces, Fig. 5 reveals that trace gas VMRs are more uniformly distributed and the probabilities vary less on PV surfaces. This indicates a more pronounced mixing state of trace gases on these surfaces rather than on isentropic surfaces.

A further coordinate system to look at the trace gas distribution and their variability is a coordinate system centred at the tropopause. Unfortunately, there was no instrument aboard the Learjet 35A measuring temperature profiles continuously along the flight track from which the tropopause altitude could be determined after the WMO definition (WMO, 1986). Anyhow, the extra-tropical tropopause during SPURT can be derived dynamically from a PV threshold value, i.e. 2 PVU. The distance from the local dynamical tropopause (ΔΘ) is therefore derived from the afore described ECMWF

analyses by taking a certain PV surface as the extra-tropical tropopause. Note, the data resulting from processing of the ECMWF analyses (e.g. PV, $\Delta\Theta$) are not identical to the data presented in Hoor et al. (2004), where higher resolved T511L60 ECMWF data were used. Nevertheless, intercomparisons evidence for a clear agreement. The meteorological analyses were interpolated to isentropic surfaces, the actual distance of the aircraft's location to the local tropopause is denoted as $\Delta\Theta$ and is given in K. To account for the strong gradient of PV in the tropopause region, several threshold values of PV were chosen as the dynamical extra-tropical tropopause ranging from 2 PVU to 6 PVU in 0.5 PVU steps. Through the different threshold values the character of the PDFs, i.e. location of high probabilities, spreading and trace gas variability, does not change seriously. Thus, for representativeness, only the O_3 and H_2O distribution for the distance to the 2 PVU surface ($\Delta\Theta_2$) for measurements during spring are shown in Fig. 6. For the distributions obtained for the other seasons as well as with $\Delta\Theta_4$ as the reference coordinate it is referred to Krebsbach (2005).

The PDFs with respect to the distance to a threshold value of PV look similar to those in the PV space. Anyhow, the use of $\Delta\Theta$ exhibits a slightly more compact shape, in particular for the campaigns in the winter and spring months (see also Sect. 4.3). The fact that the PDFs look very similar in shape and distribution of probabilities in the view of PV and $\Delta\Theta$ suggests an advanced mixing state of these trace gases on surfaces relative to the local tropopause. However, each air parcel in the atmosphere can be thought of as beeing labelled by its PV, controlling or restraining the air parcels' range of motion. A relatively huge degree of freedom is given in regions of uniform PV (Sparling and Schoeberl, 1995). Thus, spatial gradients of PV might account for the dynamical affected trace gas distributions and not solely its absolute values. And this is exactly what the PDFs for different PV threshold values for the dynamically defined extra-tropical tropopause show, since the shape and the spreading of distributions remain to the largest extent the same. This implies that the extra-tropical transition layer follows surfaces of PV or surfaces relative to the shape of the local tropopause, if defined by PV, rather than isentropic surfaces. This is consistent with the results of Hoor

et al. (2004).

4.2. Mixing entropy

A useful measure for the trace gas variability in the PDFs is, for instance, the mixing entropy, which could in general be regarded as a measure for uncertainty. For a uni-modal PDF the characterisation is reliably given by the first and second moments, e.g. mean and variance, respectively. Using these moments, the PDF is described by a relation to a single reference value, like the mean. This is probably inaccurate for a multi-modal distribution, where there is no symmetry around the reference (Sparling, 2000). A measure for the information content in a PDF for a trace gas μ provides Shannon's entropy which is given as

$$SE = -\sum_{i=1}^{N} p_i \cdot ln\, p_i\,, \tag{1}$$

with ln as the natural logarithm (e.g. Srikanth et al., 2000). Concerning a PDF with D total observed data points of trace gas μ and N bins of width $\Delta\mu$, the fraction of observation in the i^{th} cell (p_i) is the number of observations within this cell (N_i) divided by D, and $\sum_{i=1}^{N} p_i = 1$. The information content is therefore solely dependent upon a given probability distribution and does not directly relate to the content or meaning of the underlying events, i.e. the quantity of the binned trace gas. Only the probability of the occurring events is important, not the events themselves. SE is zero if the distribution has a maximum VMR, e.g. chemical homogeneity within one bin. For a uniform spatial distribution, i.e. $p_i = 1/N\ \forall i$, the considered trace gas field has a maximum variability (any observed value can be placed in any one of the N bins) and the entropy is maximal ($SE = SE_{max} = ln\, N$). A maximum entropy implies indistinguishability of the air parcels. Moreover, they have an unrestricted free range of motion. In reality, PV constrains the air parcels' range of motion. Thus, a maximum entropy value is not to be expected (Sparling and Schoeberl, 1995). The maximum entropy is dependent upon

the number of bins. For a better comparison of different entropy values, a normalisation to the maximum entropy is performed, resulting in

$$\frac{SE}{SE_{\max}} = -\sum_{i=1}^{N} p_i \cdot log_N\, p_i \leq 1\,. \quad (2)$$

The normalised mixing entropy is illustrated for O_3 and H_2O with PV as the reference coordinate above each seasonal PDF in Fig. 5. In the O_3 PDFs the normalised mixing entropy values enlarge with an increase in the coordinate value, i.e. height. In the troposphere (i.e. PV values lower than 2 PVU) the normalised mixing entropy is considerably small, indicating only small-scale and low trace gas variability. A low mixing entropy value indicates a rather homogeneous air mass. This seems a little bit strange, since a well-mixed state, as an equilibrium state, should have maximum entropy. It should be noted that SE is distinct from the thermodynamical entropy. Thus, the entropy here is considered in the "chemical space" in contrast to the "physical space" (Sparling, 2000). The PDFs show highest entropy values in the LMS for O_3 and in the troposphere as well as in the extra-tropical transition layer for H_2O. The corresponding trace gas variability is maximal in these regions, implying the occurrence of different mixing states.

In all used different coordinates, normalised mixing entropy values show a reversed course for O_3 and H_2O (for mixing entropies related to Θ, $\Delta\Theta_2$ and $\Delta\Theta_4$ see Krebsbach, 2005). Total water mixing ratios are highly variable in the troposphere, whereas ozone is comparably homogeneously distributed with respect to the bin size of the considered coordinate. Due to the strong gradient of both trace gases at or in the vicinity of the tropopause, normalised mixing entropy values increase for O_3 and decrease for H_2O with further penetration into the LMS. Therefore, at a PV value of ≈2 PVU also a strong gradient in the normalised mixing entropy is evident. During spring the O_3 variability is highest in the LMS, probably due to the enhanced downward motion. Thus, the O_3 entropy values are maximal during this season. The same arises for the enhanced H_2O content and variability in the LMS during the summer months. The seasonal trace

gas cycles are therefore also reflected by the seasonal course of the mixing entropies.

Despite the comprehensive data coverage in the UT/LMS obtained during the SPURT project, it should be mentioned that to derive a more valuable statement from the mixing entropy, considerably more measurements are required, in particular in the upper LMS.

4.3. Functional and structural correlations

A common measure for a relation between ordinal or continuous variables is the product-moment coefficient. Pearson's correlation coefficient (r) reflects the degree of linear relationship between two variables, say x and y, of dimension N. The functional correlation is defined as

$$r_{xy} = \frac{\sum_{i=1}^{N}(x_i - \bar{x})(y_i - \bar{y})}{\sqrt{\sum_{i=1}^{N}(x_i - \bar{x})^2}\sqrt{\sum_{i=1}^{N}(y_i - \bar{y})^2}}, \quad (3)$$

with $\bar{x}$ ($\bar{y}$) as the mean of the x_i's (y_i's). It can range from −1 to +1, inclusive, i.e. from a perfect negative to a perfect positive correlation, whereby r=0 indicates that x and y are uncorrelated. To decide, whether a correlation is significantly stronger than another, Pearson's r is not an accurate measure, since the individual distributions of x and y are not considered.

A more structural measure for the relationship between two variables provides Spearman's correlation coefficient (ϱ), which is a non-parametric or rank correlation. The computation is performed by replacing the value of each x_i by the value of its rank, i.e. the smallest value of variable x is converted to rank 1, the highest to rank N. The same applies for the y_i values. An outstanding advantage of the rank correlation is that a non-parametric correlation is more robust than a linear correlation, in the same sense as the median is more robust than the mean (Press et al., 1997). After convert-

ing the numbers to ranks the Spearman correlation coefficient is calculated according to Eq. (3).

In Table 1 both Pearson's and Spearman's correlation coefficients are shown for O_3 (top) versus different parameters. Ozone does not show best correlations with potential temperature. As is directly evident from both coefficients, highest positive correlations appear when O_3 is related to PV and/or to $\Delta\Theta$. The coefficients are also high for almost all chosen PV threshold values to define the local dynamical tropopause. Further, this rather simple measure for the association between two parameters reveal the conclusion drawn from the PDFs. Trace gas isopleths of O_3 seem to be orientated along surfaces of PV rather than along isentropes. The differences between r and ϱ for PV and the $\Delta\Theta$s are only small. In contrast, the correlations of O_3 with pressure are comparatively insignificant, nevertheless exhibiting larger structural negative coefficients during some winter and spring campaigns.

The correlation coefficients for H_2O versus different parameters are listed in Table 1 (bottom). When calculating Pearson's r, H_2O is best correlated with pressure. Both, p and H_2O, decrease very rapidly with height in a rather logarithmic manner. Thus, the good correlation is to be expected. This is especially evident during the summer campaigns (IOP 4 and IOP 8). Spearman's ϱ is independent on the mode or shape of the distribution, and it renders unnecessary to make assumptions on the functional relationship (Press et al., 1997). For this measure, H_2O shows, as O_3, a high degree of correlation when related to Θ, $\Delta\Theta$ and PV.

5. Conclusions

The unique, continuous and high resolution O_3 and H_2O measurements, obtained during the SPURT campaigns between November 2001 and July 2003, allow for a comprehensive view of the UT/LMS region above Europe. In the first part, seasonal cycles of O_3 and H_2O in the UT and LMS have been analysed. As indicated by extensive studies of vertical profiles obtained during ascents and descents (see Hoor et al., 2004;

Krebsbach, 2005), the tropopause location, i.e. the noticeable boundary between the troposphere and the stratosphere, coincides quite well with the 2 PVU surface. Different analyses of the trace gas measurements reveal that the seasonal cycle of O_3 in the UT shows a spring to summer maximum, most probably affected by in situ photochemistry (cf. also Hegglin et al.). In the LMS the seasonal O_3 cycle is more pronounced and shifted in phase by about 2–3 months earlier in the year, exhibiting a distinct spring time maximum. In the upper part of the LMS, a pronounced O_3 maximum is established during spring, whereas the lower part of the LMS still contains large contributions of rather O_3-poor tropospheric air during winter and early spring. Only around April the O_3 maximum is also established in the lower part. This is the effect of the large-scale stratospheric winter/spring Brewer-Dobson circulation (see also Krebsbach et al., a, and Hegglin et al.). Induced by breaking Rossby waves and strong diabatic subsidence (the downward control principle, Haynes et al., 1991) aged and O_3-rich stratospheric air is transported downward into the LMS (e.g. Austin and Follows, 1991; Beekmann et al., 1994; Logan, 1999). Thus, during spring a contribution of stratospheric O_3 due to stratosphere-to-troposphere transport is likely to affect tropospheric O_3.

In contrast to the O_3 seasonal cycles, H_2O shows no phase shift between the UT and the LMS. Maximum H_2O VMRs were observed during the summer campaigns close to the tropopause in the UT as well as in the LMS. Lowest H_2O VMRs were measured during winter and autumn, the latter indicating a temporally link with the sub-tropics/tropics (cf. Krebsbach et al., a, b). The reason for this seasonality is twofold. First, since H_2O is strongly influenced by heterogeneous processes, it follows the temperature variation at the tropopause, i.e. the air is widely freeze-dried during its transport into the LMS (see also Krebsbach et al., c). Second, whereas downward transport of dry air from the overworld into the LMS is dominant during winter, the barrier for quasi-isentropic transport of moist air over the tropopause deep into the LMS is weak during summer.

To examine the distribution, spreading, and variability of both trace gases, especially 2-dimensional probability distribution functions were used. Moreover, from these distributions, effects of transport and mixing processes can be inferred. Considering several

chemical, thermal, and dynamical coordinates, the measured trace gases show most compact distributions and best correlations when related to potential vorticity and distance to the dynamically defined tropopause. Moreover, using various PV threshold values for the extra-tropical tropopause, the distributions show almost the same shape. The trace gas isopleths follow surfaces of PV or the shape of the tropopause, in accordance with results from Hoor et al. (2004). This suggests an advanced mixing state on surfaces relative to the shape of the tropopause.

The mixing entropy is assigned to characterise the PDFs and to estimate trace gas variability. Entropy values for O_3 and H_2O in the LMS appear to be maximal during spring and summer, respectively. This indicates highest variability of these trace gases during the respective seasons with greater impact of stratospheric air during spring and tropospheric air during summer.

Acknowledgements. SPURT is an AFO 2000 project and has been funded by the German BMBF (German: Bundesministerium für Bildung und Forschung) under contract No. 07ATF27 and additionally supported by the SNF (Swiss National Fund). The authors acknowledge the ECMWF (European Centre for Medium-Range Weather Forecasts) for usage of meteorological data. We are also grateful to enviscope GmbH (Frankfurt a. M., Germany) for professional technical support and professional organisation. Further thanks are due to the pilots and the GFD (German: Gesellschaft für Flugzieldarstellung) for the excellent operation of the Learjet 35A.

References

Ancellet, G. and Beekmann, M.: Evidence for changes in the ozone concentrations in the free troposphere over southern France from 1976 to 1995, Atmos. Environ., 31, 2835–2851, 1997. 7254

Appenzeller, C., Holton, J. H., and Rosenlof, K. H.: Seasonal variation of mass transport across the tropopause, J. Geophys. Res., 101, 15 071–15 078, 1996. 7254

Austin, J. F. and Follows, M. J.: The ozone record at Payerne: An assessment of the cross-tropopause flux, Atmos. Environ., 25, 1873–1880, 1991. 7255, 7268

Beekmann, M., Ancellet, G., and Mégie, G.: Climatology of tropospheric ozone in southern

Europe and its relation to potential vorticity, J. Geophys. Res., 99, 12 841–12 853, 1994. 7252, 7254, 7256, 7268
Brennikmeijer, C. A. M., Slemr, F., Koeppel, C., Scharffe, D. S., Pupek, M., Lelieveld, J., Crutzen, P., Zahn, A., Sprung, D., Fischer, H., Hermann, M., Reichelt, M., Heintzenberg, J., Schlager, H., Ziereis, H., Schumann, U., Dix, B., Platt, U., Ebinghaus, R., Martinsson, B., Ciais, P., Filippi, D., Leuenberger, M., Oram, D., Penkett, S., van Velthoven, P., and Waibel, A.: Analyzing Atmospheric Trace Gases and Aerosols Using Passenger Aircraft, EOS, 86, 2005. 7250
Brunner, D., Staehelin, J., and Jeker, D.: Large-Scale Nitrogen Oxide Plumes in the Tropopause Region and Implications for Ozone, Science, 282, 1305–1309, 1998. 7250
Brunner, D., Staehelin, J., Jeker, D., Wernli, H., and Schumann, U.: Nitrogen oxides and ozone in the tropopause region of the Northern Hemisphere: Measurements from commercial aircraft in 1995/1996 and 1997, J. Geophys. Res., 106, 27 673–27 699, 2001. 7254
Chen, P.: Isentropic cross-tropopause mass exchange in the extratropics, J. Geophys. Res., 100, 16 661–16 673, 1995. 7255
Derwent, R. G., Simmonds, P. G., Seuring, S., and Dimmer, C.: Observation and interpretation of the seasonal cycles in the surface concentrations of ozone and carbon monoxide at Mace Head, Ireland from 1990 to 1994, Atmos. Environ., 32, 145–157, 1998. 7254
Dessler, A. E., Hintsa, E. J., Weinstock, E. M., Anderson, J. G., and Chan, K. R.: Mechanisms controlling water vapor in the lower stratosphere: "A tale of two stratospheres", J. Geophys. Res., 100, 23 167–23 172, 1995. 7257, 7258
Eluszkiewicz, J.: A three-dimensional view of the stratosphere-to-troposphere exchange in the GFDL SKYHI model, Geophys. Res. Lett., 23, 2489–2492, 1996. 7255
Engel, A., Bönisch, H., Brunner, D., Fischer, H., Franke, H., Günther, G., Gurk, C., Hegglin, M., Hoor, P., Königstedt, R., Krebsbach, M., Maser, R., Parchatka, U., Peter, T., Schell, D., Schiller, C., Schmidt, U., Spelten, N., Szabo, T., Weers, U., Wernli, H., Wetter, T., and Wirth, V.: Highly resolved observations of trace gases in the lowermost stratosphere and upper troposphere from the SPURT project: an overview, Atmos. Chem. Phys. Discuss., 5, 5081–5126, 2005,
SRef-ID: 1680-7375/acpd/2005-5-5081. 7250, 7251
Foot, J. S.: Aircraft measurements of the humidity in the lower stratosphere from 1977 to 1980 between 45° N and 65° N, Quart. J. Roy. Meteor. Soc., 110, 303–319, 1984. 7257
Good, P. and Pyle, J.: Refinements in the use of equivalent latitude for assimilating sporadic inhomogeneous stratospheric tracer observations, 1: Detecting transport of Pinatubo aerosol

across a strong vortex edge, Atmos. Chem. Phys., 4, 1823–1836, 2004, SRef-ID: 1680-7324/acp/2004-4-1823. 7252
Haynes, P. and Shepherd, T.: Report on the SPARC Tropopause Workshop, Bad Tölz, Germany, 17–21 April 2001, SPARC newsletter N. 17, 2000. 7255
Haynes, P. H., Marks, C. J., McIntyre, M. E., Sheperd, T. G., and Shine, K. P.: On the "downward control" of extratropical diabatic circulations by eddy-induced mean zonal forces, J. Atmos. Sci., 48, 651–678, 1991. 7268
Hegglin, M. I.: Airborne NO_y-, NO- and O_3-measurements during SPURT: Implications for atmospheric transport, Ph.D. thesis, Swiss Federal Institute of Technology Zürich, Diss. ETH No. 15553, 2004. 7251
Hegglin, M. I., Brunner, D., Wernli, H., Schwierz, C., Martius, O., Hoor, P., Fischer, H., Parchatka, U., Spelten, N., Schiller, C., Krebsbach, M., , Weers, U., Staehelin, J., and Peter, T.: Tracing troposphere-to-stratosphere transport above a mid-latitude deep convective system, Atmos. Chem. Phys., 4, 741–756, sRef-ID: 1680-7324/acp/2004-4-741, 2004, SRef-ID: 1680-7324/acp/2004-4-741. 7259
Hintsa, E. J., Weinstock, E. M., Dessler, A. E., Anderson, J. G., Loewenstein, M., and Podolske, J. R.: SPADE H_2O measurements and the seasonal cycle of stratospheric water vapor, Geophys. Res. Lett., 21, 2559–2562, 1994. 7257
Hintsa, E. J., Boering, K. A., Weinstock, E. M., Anderson, J. G., Gary, B. L., Pfister, L., Daube, B. C., Wofsy, S. C., Loewenstein, M., Podolske, J. R., Margitan, J. J., and Bui, T. P.: Troposhere-to-stratosphere transport in the lowermost stratosphere from measurements of H_2O, CO_2, N_2O and O_3, Geophys. Res. Lett., 25, 2655–2658, 1998. 7258
Hoinka, K. P.: Temperature, Humidity, and Wind at the Global Tropopause, Mon. Wea. Rev., 127, 2248–2265, 1999. 7257
Hollingsworth, A. and Lönneberg, P.: The verification of objective analyses: Diagnostics of analysis system performance, Met. Atmos. Phys., 40, 3–27, 1989. 7252
Holton, J. R., Haynes, P. H., McIntyre, M. E., Douglass, A. R., Rood, R. B., and Pfister, L.: Stratosphere-troposphere exchange, Rev. Geophys., 33, 403–439, 1995. 7255, 7258
Hoor, P., Gurk, C., Brunner, D., Hegglin, M. I., Wernli, H., and Fischer, H.: Seasonality and extent of extratropical TST derived from in-situ CO measurements during SPURT, Atmos. Chem. Phys., 4, 1427–1442, 2004, SRef-ID: 1680-7324/acp/2004-4-1427. 7253, 7263, 7267, 7269
Hoskins, B. J.: Towards a $PV - \theta$ view of the general circulation, Tellus, 43AB, 27–35, 1991.

7257
Hoskins, B. J., McIntyre, M. E., and Robertson, A. W.: On the use and significance of isentropic potential vorticity maps, Quart. J. Roy. Meteor. Soc., 111, 877–946, 1985. 7253
Hough, A. M.: Development of a two-dimensional global tropospheric model: Model chemistry, J. Geophys. Res., 96, 7325–7362, 1991. 7254
Inamdar, A. K. and Ramanathan, V.: Tropical and global scale interactions among water vapor, atmospheric greenhouse effect, and surface temperature, J. Geophys. Res., 103, 32 177–32 194, 1998. 7249
Krebsbach, M.: Trace gas transport in the UT/LS: seasonality, stratosphere-troposphere exchange and implications for the extra-tropical mixing layer derived from airborne O_3 and H_2O measurements, Ph.D. thesis, Bergische Universität Wuppertal, urn:nbn:de:hbz:468-20050180, 2005. 7253, 7254, 7257, 7258, 7260, 7261, 7263, 7265, 7268
Lindzen, R. S.: Some Coolness Concerning Global Warming, Bull. Am. Met. Soc., 71, 288–299, 1990. 7249
Liu, S. C., Trainer, M., Fehsenfeld, F., Parrish, D., Williams, E. J., Fahey, D. W., Hübler, G., and Murphy, P. C.: Ozone production in the rural troposphere and the implications for regional and global ozone distributions, J. Geophys. Res., 92, 4191–4207, 1987. 7255
Logan, J.: Tropospheric ozone: Seasonal behaviour, trends and anthropogenic influence, J. Geophys. Res., 90, 10 463–10 482, 1985. 7254, 7255
Logan, J.: Ozone in rural areas of the United States, J. Geophys. Res., 94, 8511–8532, 1989. 7254
Logan, J. A.: An analysis of ozonesonde data for the lower stratosphere: Recommendations for testing models, J. Geophys. Res., 104, 16 151–16 170, 1999. 7254, 7255, 7268
Marenco, A., Válerie, T., Nédélec, P., Smit, H., Helten, M., Kley, D., Karcher, F., Simon, P., Law, K., Pyle, J., Poschmann, G., von Wrede, R., Hume, C., and Cook, T.: Measurement of ozone and water vapor by Airbus in-service aircraft: The MOZAIC airborne program, An overview, J. Geophys. Res., 103, 25 631–25 642, 1998. 7250
Mastenbrook, H. J. and Oltmans, H. J.: Stratospheric Water Vapor Variability for Washington, DC/Boulder, CO: 1964–82, J. Atmos. Sci., 40, 2157–2165, 1983. 7257
McLinden, C. A., Olsen, S. C., Hannegan, B., Wild, O., Prather, M. J., and Sundet, J.: Stratospheric ozone in 3-D models: A simple chemistry and the cross-tropopause flux, J. Geophys. Res., 105, 14 653–14 665, 2000. 7249
Monks, P. S.: A review of the observations and origins of the spring ozone maximum, Atmos.

Environ., 34, 3545–3561, 2000. 7254
Mottaghy, D.: Ozonmessungen in der unteren Stratosphäre, Master's thesis, Rheinisch-Westfälische Technische Hochschule Aachen, in cooperation with the Institute for Chemistry and Dynamics of the Geosphere, ICG-I: Stratosphere, 2001. 7251
Nedoluha, G. E., Bevilacqua, R. M., Hoppel, K. W., Lumpe, J. D., and Smit, H.: Polar Ozone and Aerosol Measurement III measurements of water vapor in the upper troposphere and lowermost stratosphere, J. Geophys. Res., 107, doi:10.1029/2001JD000 793, 2002. 7249, 7257
Oltmans, S. J. and Hofmann, D. J.: Increase in lower-stratospheric water vapour at a mid-latitude Northern Hemisphere site from 1981 to 1994, Nature, 374, 146–149, 1995. 7257
Oltmans, S. J. and Levy II, H.: Surface ozone measurements from a global network, Atmos. Environ., 28, 9–24, 1994. 7255
Pan, L., Solomon, S., Randel, W., Lamarque, J.-F., Hess, P., Gille, J., Chiou, E.-W., and McCormick, M. P.: Hemispheric asymmetries and seasonal variations of the lowermost stratospheric water vapor and ozone derived from SAGE II data, J. Geophys. Res., 102, 28 177–28 184, 1997. 7249, 7255, 7257, 7258
Pan, L. L., Hintsa, E. J., Stone, E. M., Weinstock, E. M., and Randel, W. J.: The seasonal cycle of water vapor and saturation vapor mixing ratio in the extratropical lowermost stratosphere, J. Geophys. Res., 105, 26 519–26 530, 2000. 7249, 7258
Park, M., Randel, W. J., Kinnison, D. E., and Gracia, R. R.: Seasonal variation of methane, water vapor, and nitrogen oxides near the tropopause: Satellite observations and model simulations, J. Geophys. Res., 109, doi:10.1029/2003JD003 706, 2004. 7249
Prados, A. I., Nedoluha, G. E., Bevilacqua, R. M., Allen, D. R., Hoppel, K. W., and Marenco, A.: POAM III ozone in the upper troposphere and lowermost stratosphere: Seasonal variability and comparisons to aircraft observations, J. Geophys. Res., 108, doi:10.1029/2002JD002 819, 2003. 7249, 7255, 7258
Press, W. H., Teukolsky, S. A., Vetterling, W. T., and Flannery, B. P.: Numerical Recipies in Fortran 77: The Art of Scientific Computing, vol. 1 of "Fortran Numerical Recipies", Press Syndicate of the University of Cambridge, The Pitt Building, Trumpington Street. Cambridge CB2 1RP, 2nd edn., ISBN 0-521-43064-X, 1997. 7266, 7267
Randel, W. J., Wu, F., Gettelman, A., Russell III, J. M., Zawodny, J. M., and Oltmans, S. J.: Seasonal variation of water vapor in the lower stratosphere observed in Halogen Occultation Experiment data, J. Geophys. Res., 106, 14 313–14 325, 2001. 7249

Ray, E. A., Moore, F. L., Elkins, J. W., Dutton, G. S., Fahey, D. W., Vömel, H., Oltmans, S. J., and Rosenlof, K. H.: Transport into the Northern Hemisphere lowermost stratosphere revealed by in situ tracer measurements, J. Geophys. Res., 104, 26 565–26 580, 1999. 7255

Ray, E. A., Rosenlof, K. H., Richard, E., Parrish, D., and Jakoubek, R.: Distributions of ozone in the region of the subtropical jet: An analysis of in situ aircraft measurements, J. Geophys. Res., 109, doi:10.1029/2003JD004 143, 2004. 7259

Rind, D., Chiou, E.-W., Chu, W., Larsen, J., Oltmans, S., Lerner, J., McCormick, M. P., and McMaster, L.: Positive water vapour feedback in climate models confirmed by satellite data, Nature, 349, 500–502, 1991. 7249

Scheel, H. E., Areskoug, H., Geiß, H., Gomiscek, B., Granby, K., Haszpra, L., Klasinc, L., Kley, D., Laurila, T., Lindskog, A., Roemer, M., Schmitt, R., Simmonds, P., Solberg, S., and Toupance, G.: On the Spatial Distribution and Seasonal Variation of Lower-Troposphere Ozone over Europe, J. Atmos. Chem., 28, 11–28, 1997. 7254

Schmitt, R. and Volz-Thomas, A.: Climatology of Ozone, PAN, CO, and NMHC in the Free Troposphere Over the Southern North Atlantic, J. Atmos. Chem., 28, 245–262, 1997. 7254

Sparling, L. C.: Statistical perspectives on stratospheric transport, Rev. Geophys., 38, 417–436, 2000. 7264, 7265

Sparling, L. C. and Schoeberl, M. R.: Mixing entropy analysis of dispersal of aircraft emissions in the lower stratosphere, J. Geophys. Res., 100, 16 805–16 812, 1995. 7263, 7264

Sprenger, M. and Wernli, H.: A northern hemispheric climatology of cross-tropopause exchange for the ERA15 time period (1979–1993), J. Geophys. Res., 108, doi:10.1029/2002JD002 636, 2003. 7261

Srikanth, M., Kesavan, H. K., and Roe, P. H.: Probability Density Function Estimation using the MinMax Measure, IEEE Transactions on Systems, Man, and Cybernetics – Part C: Applications and Reviews, 30, 77–83, 2000. 7264

Stone, E. M., Pan, L., Sandor, B. J., Read, W. G., and Waters, J. W.: Spatial distributions of upper tropospheric water vapor measurements from the UARS Microwave Limb Sounder, J. Geophys. Res., 105, 12 149–12 161, 2000. 7249, 7257

Strahan, S. E.: Climatologies of lower stratospheric NO_y and O_3 and correlations with N_2O based on in situ observations, J. Geophys. Res., 104, 30 463–30 480, 1999. 7250

Wang, P.-H., Cunnold, D. M., Zawodny, J. M., Pierce, R. B., Olson, J. R., Kent, G. S., and Skeens, K. M.: Seasonal ozone variations in the isentropic layer between 330 and 380 K as observed by SAGE II: Implications of extratropical cross-tropopause transport, J. Geophys.

Res., 103, 28 647–28 659, 1998. 7255
WMO: Atmospheric Ozone 1985, WMO Global Ozone Res. and Monit. Proj. Rep. 20, Geneva, 1986. 7262
Zahn, A., Brenninkmeijer, C. A. M., and van Velthoven, P. F. J.: Passenger aircraft project CARIBIC 1997-2002, Part II: the ventilation of the lowermost stratosphere, Atmos. Chem. Phys. Discuss., 4, 1119–1150, 2004,
SRef-ID: 1680-7375/acpd/2004-4-1119. 7256
Zöger, M., Afchine, A., Eicke, N., Gerhards, M.-T., Klein, E., McKenna, D. S., Mörschel, U., Schmidt, U., Tan, V., Tuitjer, F., Woyke, T., and Schiller, C.: Fast in situ stratospheric hygrometers: A new family of balloon-borne and airborne Lyman α photofragment fluorescence hygrometers, J. Geophys. Res., 104, 1807–1816, 1999. 7251

Table 1. Pearson's r (left) and Spearman's rank ϱ (right) correlation coefficients for O_3 (top) and H_2O (bottom) versus potential temperature (Θ), potential vorticity (PV), distance to the local dynamically defined tropopause (i.e. 2, 3, 4 PVU surface, $\Delta\Theta_2$, $\Delta\Theta_3$, $\Delta\Theta_4$, respectively), and pressure (p). The coefficients of the eight single SPURT campaigns (IOP 1–8) are given for the two campaigns in each season, as incdicated by the corresponding month and year (mm/yy). Best correlation coefficients (negative or positive) are highlighted in bold.

IOPs: mm/yy	functional correlation Pearson r: O_3 vs.						structural correlation Spearman ϱ: O_3 vs.					
	Θ	PV	$\Delta\Theta_2$	$\Delta\Theta_3$	$\Delta\Theta_4$	p	Θ	PV	$\Delta\Theta_2$	$\Delta\Theta_3$	$\Delta\Theta_4$	p
1, 5: 11/01, 10/02	0.58	**0.87**	0.85	0.85	0.85	−0.29	0.59	0.90	0.89	0.90	**0.90**	−0.23
2, 6: 01/02, 02/03	0.80	0.86	0.91	**0.92**	0.91	−0.49	0.82	0.91	0.93	**0.94**	0.93	−0.55
3, 7: 05/02, 04/03	0.82	0.91	**0.93**	0.93	0.92	−0.50	0.84	0.92	**0.94**	0.94	0.93	−0.48
4, 8: 08/02, 07/03	0.47	**0.84**	0.76	0.78	0.80	−0.27	0.47	**0.89**	0.80	0.84	0.87	−0.25
	Pearson r: H_2O vs.						Spearman ϱ: H_2O vs.					
	Θ	PV	$\Delta\Theta_2$	$\Delta\Theta_3$	$\Delta\Theta_4$	p	Θ	PV	$\Delta\Theta_2$	$\Delta\Theta_3$	$\Delta\Theta_4$	p
1, 5: 11/01, 10/02	−0.50	−0.45	−0.43	−0.44	−0.45	**0.70**	−0.79	−0.72	**−0.82**	−0.82	−0.81	0.57
2, 6: 01/02, 02/03	−0.46	−0.49	−0.43	−0.43	−0.44	**0.70**	−0.55	**−0.60**	−0.56	−0.54	−0.54	0.60
3, 7: 05/02, 04/03	−0.46	−0.47	−0.39	−0.39	−0.39	**0.67**	**−0.67**	−0.62	−0.62	−0.61	−0.59	0.55
4, 8: 08/02, 07/03	−0.60	−0.50	−0.50	−0.47	−0.44	**0.72**	**−0.81**	−0.64	−0.75	−0.72	−0.66	0.72

ACPD
5, 7247–7282, 2005

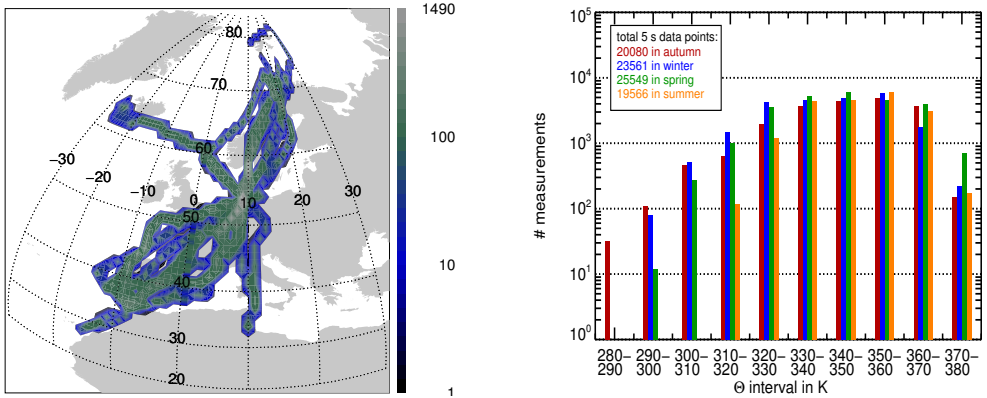

Fig. 1. Distributions of obtained O_3 and/or H_2O measurements during SPURT. In the map (left), the number of 5 s data points in a 1° longitude × 1° latitude grid is displayed. The colour bar reflects the number of data points in each geographical bin. The right chart shows frequency distributions of the same data in the potential temperature space, binned in 10 K steps. By this approach, a seasonal separation is performed (autumn, winter, spring, and summer, corresponding to red, blue, green, and orange, respectively). The total number of merged data points within the considered Θ range in each season is given in the upper left corner.

ACPD
5, 7247–7282, 2005

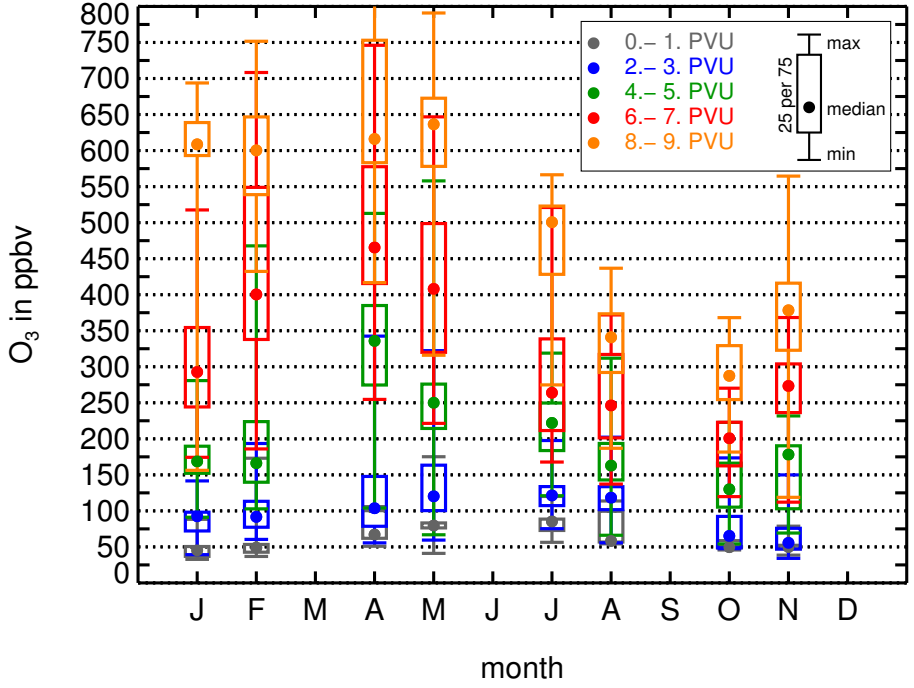

Fig. 2. Annual cycles of ozone mixing ratios in ppbv in the region of the upper troposphere and lowermost stratosphere as derived from the SPURT measurements. The measurements are displayed as box plots in terms of potential vorticity, noncontinuously incremented by 1 PVU due to facility of inspection (colour coding for 0–1, 2–3, 4–5, 6–7, 8–9 PVU), as indicated in the upper right corner. The median in each PV interval is represented by a dot, the box reflects the 25 and 75 percentiles, and the whiskers indicate minimum and maximum O_3 VMRs.

ACPD
5, 7247–7282, 2005

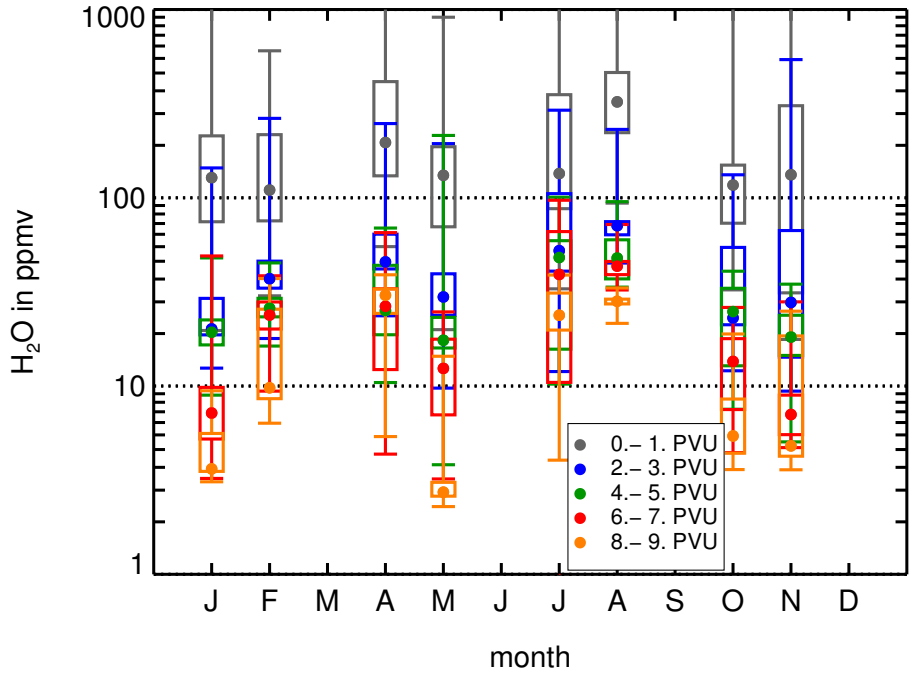

Fig. 3. As Fig. 2, but for total water mixing ratios (in ppmv).

ACPD
5, 7247–7282, 2005

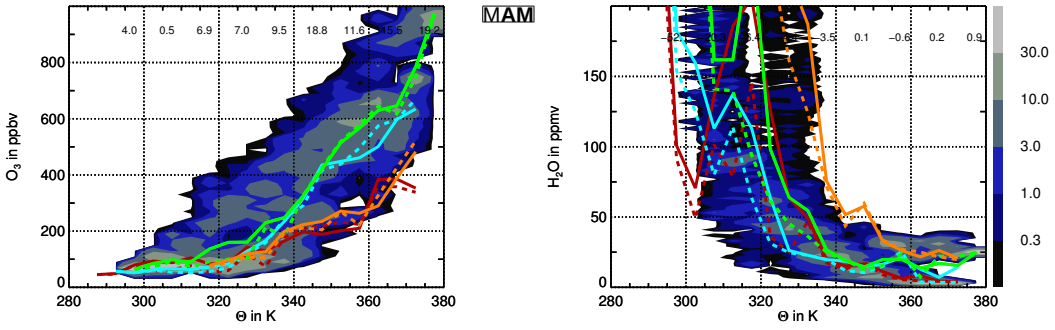

Fig. 4. Seasonal 2-dimensional probability distribution functions of O_3 (left) and H_2O (right) as a function of the thermal coordinate Θ for the spring measurements. The bin size is 20 ppbv for O_3, 2 ppmv for H_2O, and 5 K for Θ. The normalisation is performed to each Θ bin, i.e. the probability (colour coding) reflects the percentage of an observed trace gas VMR in a single Θ interval. In both panels the mean and the median trace gas mixing ratio in each particular Θ interval is given by the solid and dashed line, respectively. In addition, the derived means and medians for each season are compared (red, blue, green, orange corresponding to autumn, winter, spring, summer). Moreover, in the PDFs the trace gas gradients in dependence of the thermal coordinate are calculated for a doubled bin size, indicated by the top numbers.

ACPD
5, 7247–7282, 2005

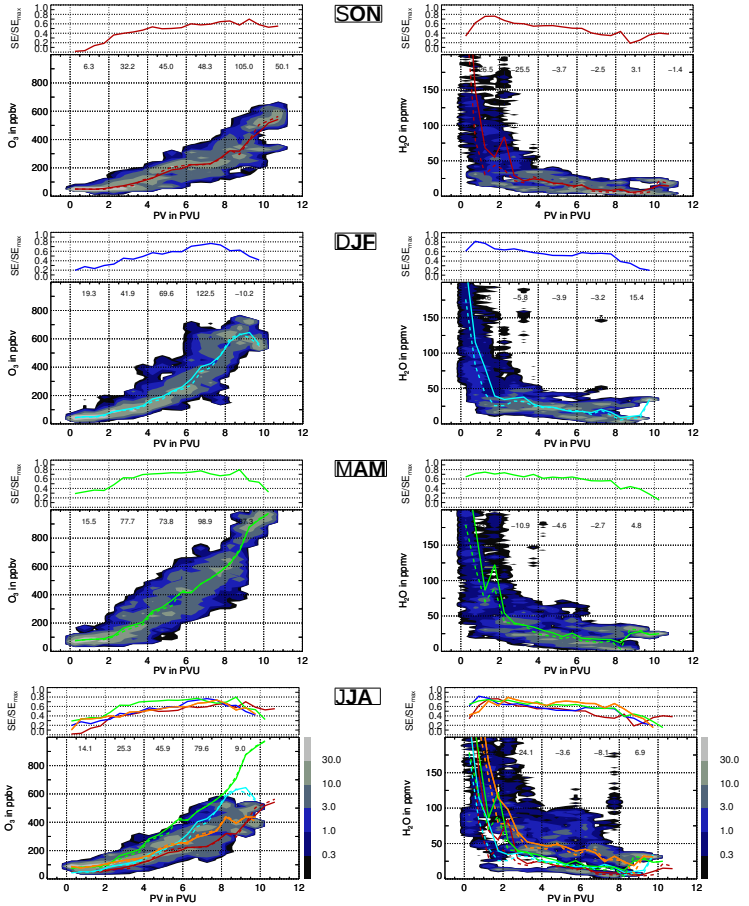

Fig. 5. As Fig. 4, but for all seasons and as a function of the dynamical coordinate PV. The bin size for PV is set to 0.5 PVU. In the top panel of the PDFs the normalised mixing entropy in each PV bin is displayed (see Sect. 4.2), also seasonally compared in the bottom charts. From top to bottom: autumn, winter, spring, and summer.

ACPD
5, 7247–7282, 2005

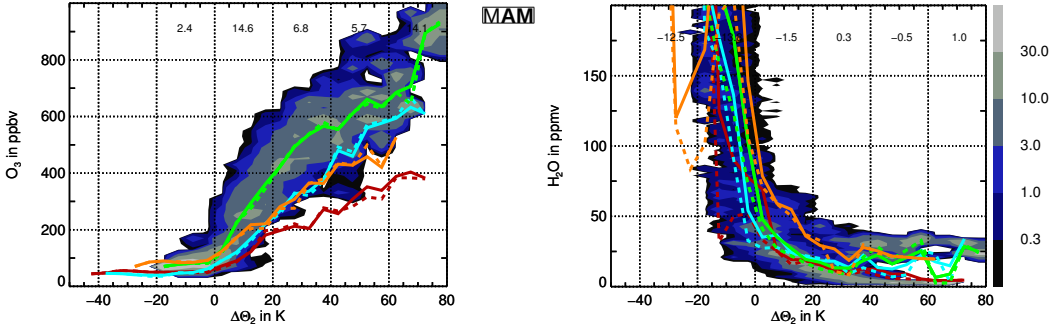

Fig. 6. As Fig. 4, but related to the distance to the local tropopause in K, considered as the 2 PVU surface. The bin size for $\Delta\Theta_2$ is 5 K.

ACPD
5, 7247–7282, 2005